General characterization of qubit-preserving impairments on two-qubit Bell nonlocality

Richard A. Brewster,[1,*] Gerald Baumgartner,[2] and Yanne K. Chembo[1]

[1]*University of Maryland, A. James Clark School of Engineering, Department of Electrical and Computer Engineering & Institute for Research in Electronics and Applied Physics (IREAP), 8279 Paint Branch Dr, College Park, Maryland 20742, USA*

[2]*Laboratory for Telecommunication Sciences, 8080 Greenmead Drive, College Park, Maryland 20740, USA*

(Received 30 August 2022; accepted 9 February 2023; published 27 February 2023)

A general technique for experimentally characterizing the effect of qubit-preserving impairments on the Clauser-Horne-Shimony-Holt parameter is introduced. This technique is independent of the underlying qubit encoding and is theoretically demonstrated for specific example impairments in polarization-encoded quantum-optical qubits. Included in this analysis is how spectrotemporal impairments can be incorporated into this technique.

DOI: 10.1103/PhysRevA.107.022225

I. INTRODUCTION

Entanglement [1–3] is a vital resource in the field of quantum information. In quantum communications, entanglement may be used for guaranteed secure communication [4] or the transfer of quantum information through the process of quantum teleportation [5]. Robust entanglement may be distributed throughout a quantum network using the process of entanglement swapping [6]. Furthermore, entangled states are a typical desired output from a controlled NOT (CNOT) operation in quantum computing [7–9].

Much like any informational resource in a real-world physical system, entanglement is subject to system impairments. Nonideal experimental components can reduce the quality of entanglement resources, which may result in errors in quantum information processing protocols. It is therefore desirable to have a means to characterize the quality of entanglement in a system. Such characterization would ensure that the quality of an entangled system is sufficient for the relevant protocols before quantum information resources are committed.

To this end, many entanglement measures have been developed to gauge the quality of entanglement in a system [3,10–14]. However, in order to experimentally compute most of these entanglement measures, full-state quantum tomography is required [3,15,16]. Such measurements require expending extensive amounts of a quantum resource, which may be undesirable in a real-world system. This issue may be mitigated to some extent by considering entanglement witnesses [3,11,17–21]. However, entanglement witnesses need to be tailored to specific classes of entangled states, which may not be feasible in complicated quantum networks. Nonlinear [3,22] or collective [3,23] witnesses may be used to improve the performance of entanglement witnesses; however, entanglement witnesses are also predominately focused on confirming the presence of entanglement and not characterizing its quality.

Another potential solution that is relatable to entanglement witnesses is a measurement of the nonlocality [2,24–26] of a state. Nonlocality can be measured through the well-known Bell inequality violation experiments [27]. One example of such an experiment is the Clauser-Horne-Shimony-Holt (CHSH) measurement [28] shown in Fig. 1(a). This experiment requires only four experimental trials with N measurements in each trial. An equivalent quantum full-state tomography measurement would require fifteen trials, again with each trial having N measurements [29]. Thus, a CHSH measurement would vastly reduce the quantum resources required compared to the entanglement measures discussed above.

The result of a single CHSH experiment is the measurable CHSH parameter S. Classical theory dictates that any given CHSH parameter must be $S \leqslant 2$ [28]. However, the principles of quantum mechanics allow for $S \leqslant 2\sqrt{2}$ [30]. Thus, when a CHSH parameter is found to be $S > 2$, the measured input state could not have been predicted by a local hidden variable theory [27,28]. Such results in the absence of loopholes are of interest because of their implications on testing local realism [31]. A continuum of S values between 2 and $2\sqrt{2}$ exists that may be used to characterize nonlocality.

Nonlocality has been demonstrated to be equivalent to entanglement measures for pure states [32,33]. It has also been related to entanglement measures for certain classes of mixed states [33–35]. Additionally, nonlocality has been demonstrated to place an upper bound on the fidelity of quantum teleportation experiments [36]. Therefore, for the purposes of this work, we will let nonlocality be an approximate measure of entanglement.

Depending on the settings of the components of the CHSH measurement, we may not achieve the maximum possible value for the CHSH parameter that exists for the underlying physical system. The optimal value $S = S_{\max}$ that is given by the ideal settings for a specified quantum state is the one that is directly related to the measure of the nonlocality of the system [25]. That is, if we consider $S_{\max}$, we have that

*Corresponding author: rbrew1@umd.edu

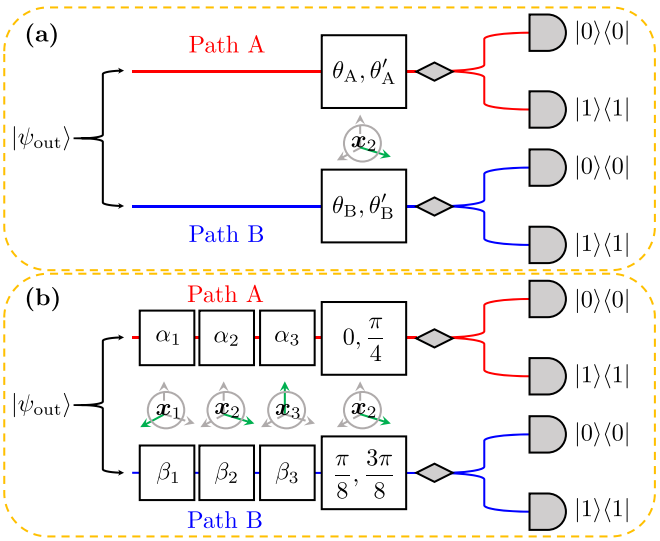

FIG. 1. Setups to measure a CHSH parameter for a state $|\psi_{\text{out}}\rangle$ subject to experimental impairments. These setups are independent of the underlying qubit encoding. The boxes represent rotations by the angles shown about the axes $\boldsymbol{x}_j$ $j \in \{1, 2, 3\}$ of the corresponding Bloch sphere. The gray diamonds denote spatially splitting the qubit according to its computational basis, which are received by the measurement devices as shown. Coincidence counts are recorded between pairs of measurements according to a typical CHSH measurement. (a) The usual CHSH experiment. The angles θ_A, θ'_A, θ_B, and θ'_B are the usual Bell test angles. This experiment is repeated four times for each possible combination of the angles used in the two paths. These angles are allowed to vary to yield the maximum possible CHSH parameter. (b) A CHSH experiment where we have fixed the Bell test angles to those shown. We have additional angles α_j, β_j, $j \in \{1, 2, 3\}$ that are about each of the corresponding axes of the Bloch sphere. These angles are adjusted to yield the maximum possible CHSH parameter given the fixed Bell test angles shown.

$S_{\max} = 2$ for a product state [32] and $S_{\max} = 2\sqrt{2}$ for a maximally entangled state [37,38].

It is therefore desired to find this optimal value. While these settings are known for certain classes of states [39], they are difficult to find for general states and/or without knowledge of the underlying physical system. One must then experimentally search for the optimal angles in general, which would limit the advantages of nonlocality outlined above. Recently, the problem has met with some interest, where machine learning has been used to perform this optimization [40,41]. As we shall demonstrate in the following section, this problem can also be mitigated to some extent by introducing the technique of Fig. 1(b) along with classical alignment. The two experiments of Fig. 1 depend on the same physical parameters, allowing for a more efficient means of measuring the nonlocality of the underlying physical system.

In this paper, we will completely characterize the optimal CHSH parameter $S_{\max}$ in the presence of qubit-preserving impairments. We will introduce the concept of a qubit-preserving impairment in the following section. As discussed, we will also demonstrate the experimental advantages of the technique of Fig. 1(b). While this technique is independent of the underlying qubit encoding, we will also theoretically demonstrate the optimal CHSH parameter in the presence of qubit-preserving impairments that affect qubits encoded in the polarization degree of freedom for single photons. This analysis will further demonstrate the usefulness of the technique of Fig. 1(b), and also gives an example for how the more complicated spectrotemporal impairments affecting photons can be incorporated into this technique.

This paper is structured as follows. In Sec. II, we provide the theoretical framework for achieving the optimal CHSH parameter of the two experiments of Fig. 1. We also demonstrate the relationship between these two experiments. In Sec. III, we provide an example of the reductions to the CHSH parameter found in polarization-encoded quantum-optical qubits. These reductions due to polarization misalignments are described in Sec. III A, spectrotemporal impairments in Sec. III B, and white noise in Sec. III C. Finally, remarks and conclusions are given in Sec. IV.

II. THEORETICAL DESCRIPTION

Before we characterize the qubit-preserving impairments of a CHSH inequality violation, we first need to define what we mean by an impairment that is qubit preserving. First, consider a system that is represented by a quantum state in an arbitrary dimensional Hilbert space. However, it is desired to approximate this state as being a member of a two-qubit (or four-dimensional) Hilbert space. A general impairment is an undesired transformation to this two-qubit state that could result from nonideal experimental components or noisy transmission lines, for example. We then define a qubit-preserving impairment as a transformation to the state such that the two-qubit basis approximation of the output state remains valid. As we shall see in the following section, many important impairments in the CHSH experiment can be characterized as qubit preserving. The effect of most qubit-preserving impairments, which include misalignments, can be calculated using unitary transformations to the quantum state. However, noise can also be qubit preserving, but cannot be represented as a unitary transformation, and its detrimental effects on a quantum system must be calculated using a density operator.

Not all impairments in a system are qubit preserving. An impairment that is not qubit preserving will transform the state in such a way that the resulting interference in the full Hilbert space, outside of the two-qubit basis, cannot be removed. An example of this situation would be multiple pair generation without number-resolving detectors [42–44]. In this case, the additional photons will negatively impact the resulting CHSH parameter even in the ideal case. In the present article, we will focus solely on qubit-preserving impairments.

We will represent a general qubit in the computational basis $|0\rangle$ and $|1\rangle$ using the vectors

$$|0\rangle \equiv \begin{pmatrix} 1 \\ 0 \end{pmatrix} \text{ and } |1\rangle \equiv \begin{pmatrix} 0 \\ 1 \end{pmatrix}. \tag{1}$$

We note that this representation is independent of the underlying physical system and holds for all orthonormal qubit encodings such as photon polarization or

path, and electron spin. It also approximately holds for pseudo-orthonormal bases such as time/frequency bins and Schrödinger cat states so long as the overlap between the respective time/frequency bins or composite coherent states is negligible.

In order to achieve a general characterization of qubit-preserving impairments on the CHSH parameter, we need to have a geometric description of a two-qubit state. This is sufficient because qubit-preserving impairments preserve the two-qubit approximation as stated above. It is well known that a single-qubit density operator $\hat{\rho}_1$ in the basis of Eq. (1) can be geometrically represented in the Bloch sphere using the Bloch vector $\boldsymbol{a}$ as [29]

$$\hat{\rho}_1 = \tfrac{1}{2}(\hat{\mathbb{1}} + \boldsymbol{a}\cdot\hat{\boldsymbol{\sigma}}), \tag{2}$$

where $\hat{\mathbb{1}}$ is the single-qubit identity operator and $\hat{\boldsymbol{\sigma}}$ is the Pauli vector

$$\begin{aligned}\hat{\boldsymbol{\sigma}} &\equiv \hat{\sigma}_1\boldsymbol{x}_1 + \hat{\sigma}_2\boldsymbol{x}_2 + \hat{\sigma}_3\boldsymbol{x}_3 \\ &= \begin{pmatrix}0 & 1\\ 1 & 0\end{pmatrix}\boldsymbol{x}_1 + \begin{pmatrix}0 & -i\\ i & 0\end{pmatrix}\boldsymbol{x}_2 + \begin{pmatrix}1 & 0\\ 0 & -1\end{pmatrix}\boldsymbol{x}_3,\end{aligned} \tag{3}$$

with the $\boldsymbol{x}_j$ corresponding to the $\mathbb{R}^3$ unit vectors. This concept can be extended for a two-qubit state $\hat{\rho}$ as [45]

$$\hat{\rho} = \frac{1}{4}\left(\hat{\mathbb{1}}\otimes\hat{\mathbb{1}} + \boldsymbol{a}\cdot\hat{\boldsymbol{\sigma}}\otimes\hat{\mathbb{1}} + \hat{\mathbb{1}}\otimes\boldsymbol{b}\cdot\hat{\boldsymbol{\sigma}} + \sum_{j=1}^{3}\sum_{k=1}^{3} T_{jk}\hat{\sigma}_j\otimes\hat{\sigma}_k\right), \tag{4}$$

where $\boldsymbol{a}$ and $\boldsymbol{b}$ are two independent Bloch vectors, one for each qubit, and the T_{jk} form the elements of the 3×3 matrix $\mathbf{T}$, which describes the correlations between the two qubits. The elements that comprise $\boldsymbol{a}$, $\boldsymbol{b}$, and $\mathbf{T}$ must be real. By construction, the operator $\hat{\rho}$ of Eq. (4) has $\mathrm{Tr}(\hat{\rho}) = 1$ and $\hat{\rho} = \hat{\rho}^\dagger$. However, the operator $\hat{\rho}$ is a density operator corresponding to a physical system if and only if it is positive semidefinite [46], which is not guaranteed.

We now consider the symmetric matrix $\mathbf{V} = \mathbf{T}^\top\mathbf{T}$. This matrix has real eigenvalues v_1, v_2, and v_3 in order of descending magnitude. It has previously been shown that the maximum possible measurable CHSH parameter $S_{\max}$ is [45]

$$S_{\max} = 2\sqrt{v_1 + v_2}. \tag{5}$$

Thus, a CHSH inequality can be violated if and only if $v_1 + v_2 > 1$ [45]. Inspection of Eq. (5) reveals that the impairments that affect the optimal CHSH parameter can only contribute to its reduction through the two eigenvalues v_1 and v_2.

The value of the CHSH parameter of Eq. (5) is found by varying the Bell test angles θ_{A}, θ'_{A}, θ_{B}, and θ'_{B} of Fig. 1(a). For a general two-qubit state, finding the specific Bell test angles that yield the maximum value is analytically challenging. Typically, one desires a Bell state in a given measurement basis. It is well known that the Bell test angles that give the maximum CHSH parameter for a Bell state are

$$\theta_{\mathrm{A}} = 0, \quad \theta'_{\mathrm{A}} = \frac{\pi}{4}, \quad \theta_{\mathrm{B}} = \frac{\pi}{8}, \quad \text{and} \quad \theta'_{\mathrm{B}} = \frac{3\pi}{8}. \tag{6}$$

We refer to these angles as the canonical Bell test angles.

In what follows, we will fix the Bell test angles to those of Eq. (6). It is important to note that, upon doing this and given the influence of the impairments in the system on the quantum state, it will likely not be possible to achieve the $S_{\max}$ of Eq. (5). We now consider the experimental situation of Fig. 1(b). Here, we have introduced angles α_j for path A and β_j for path B with $j \in \{1, 2, 3\}$. These angles, which we refer to as the optimization angles, remain fixed throughout the course of the experiment. They are adjusted to yield the maximum possible CHSH parameter given the canonical Bell test angles of Eq. (6). We denote this CHSH parameter as S_{canon}, and we have that $S_{\mathrm{canon}} \leqslant S_{\max}$. Despite this fact, we will see that there is some merit to considering this CHSH parameter.

We find S_{canon} of Fig. 1(b) by following a similar procedure to the one used in Ref [45] to obtain Eq. (5). It can be shown that, given the Bell test angles of Eq. (6), the general CHSH parameter is given by the expectation value

$$S = \sqrt{2}\langle\hat{\sigma}_1\otimes\hat{\sigma}_1 + \hat{\sigma}_3\otimes\hat{\sigma}_3\rangle = \sqrt{2}(T_{11} + T_{33}), \tag{7}$$

where the right-hand side follows from Eq. (4).

Next, we consider the rotations by the angles α_j and β_j of Fig. 1(b). We apply these angles to the observable in Eq. (7) using the Heisenberg picture. The rotations apply the unitary operator $\hat{\mathsf{U}}(\alpha_1,\alpha_2,\alpha_3)\otimes\hat{\mathsf{U}}(\beta_1,\beta_2,\beta_3)$, where $\hat{\mathsf{U}}(\alpha_1,\alpha_2,\alpha_3) = \hat{\mathsf{U}}_3(\alpha_3)\hat{\mathsf{U}}_2(\alpha_2)\hat{\mathsf{U}}_1(\alpha_1)$ and

$$\hat{\mathsf{U}}_1(\alpha) = \begin{pmatrix}\cos\alpha & i\sin\alpha\\ i\sin\alpha & \cos\alpha\end{pmatrix}, \quad \hat{\mathsf{U}}_2(\alpha) = \begin{pmatrix}\cos\alpha & -\sin\alpha\\ \sin\alpha & \cos\alpha\end{pmatrix},$$
$$\hat{\mathsf{U}}_3(\alpha) = \begin{pmatrix}e^{i\alpha} & 0\\ 0 & e^{-i\alpha}\end{pmatrix}. \tag{8}$$

This gives

$$\begin{aligned}S_{\mathrm{canon}} = \sqrt{2}\langle&\hat{\mathsf{U}}^\dagger(\alpha_1,\alpha_2,\alpha_3)\hat{\sigma}_1\hat{\mathsf{U}}(\alpha_1,\alpha_2,\alpha_3)\\ &\otimes\hat{\mathsf{U}}^\dagger(\beta_1,\beta_2,\beta_3)\hat{\sigma}_1\hat{\mathsf{U}}(\beta_1,\beta_2,\beta_3)\\ &+\hat{\mathsf{U}}^\dagger(\alpha_1,\alpha_2,\alpha_3)\hat{\sigma}_3\hat{\mathsf{U}}(\alpha_1,\alpha_2,\alpha_3)\\ &\otimes\hat{\mathsf{U}}^\dagger(\beta_1,\beta_2,\beta_3)\hat{\sigma}_3\hat{\mathsf{U}}(\beta_1,\beta_2,\beta_3)\rangle.\end{aligned} \tag{9}$$

It can be shown that

$$\begin{aligned}&\hat{\mathsf{U}}^\dagger(\alpha_1,\alpha_2,\alpha_3)\hat{\sigma}_1\hat{\mathsf{U}}(\alpha_1,\alpha_2,\alpha_3)\\ &\quad= \cos 2\alpha_2\cos 2\alpha_3\hat{\sigma}_1 + (\sin 2\alpha_1\sin 2\alpha_2\cos 2\alpha_3\\ &\qquad-\cos 2\alpha_1\sin 2\alpha_3)\hat{\sigma}_2\\ &\qquad+(\cos 2\alpha_1\sin 2\alpha_2\cos 2\alpha_3 + \sin 2\alpha_1\sin 2\alpha_3)\hat{\sigma}_3,\\ &\hat{\mathsf{U}}^\dagger(\alpha_1,\alpha_2,\alpha_3)\hat{\sigma}_2\hat{\mathsf{U}}(\alpha_1,\alpha_2,\alpha_3)\\ &\quad= -\cos 2\alpha_2\sin 2\alpha_3\hat{\sigma}_1 - (\sin 2\alpha_1\sin 2\alpha_2\sin 2\alpha_3\\ &\qquad+\cos 2\alpha_1\cos 2\alpha_3)\hat{\sigma}_2\\ &\qquad-(\cos 2\alpha_1\sin 2\alpha_2\sin 2\alpha_-\sin 2\alpha_1\cos 2\alpha_3)\hat{\sigma}_3,\\ &\hat{\mathsf{U}}^\dagger(\alpha_1,\alpha_2,\alpha_3)\hat{\sigma}_3\hat{\mathsf{U}}(\alpha_1,\alpha_2,\alpha_3)\\ &\quad= -\sin 2\alpha_2\hat{\sigma}_1 + \sin 2\alpha_1\cos 2\alpha_2\hat{\sigma}_2 + \cos 2\alpha_1\cos 2\alpha_2\hat{\sigma}_3.\end{aligned} \tag{10}$$

Thus, if we define the rotation matrix

$$\mathbf{R}(\alpha_1, \alpha_2, \alpha_3) \equiv \begin{pmatrix} \cos 2\alpha_2 \cos 2\alpha_3 & \sin 2\alpha_1 \sin 2\alpha_2 \cos 2\alpha_3 - \cos 2\alpha_1 \sin 2\alpha_3 & \cos 2\alpha_1 \sin 2\alpha_2 \cos 2\alpha_3 + \sin 2\alpha_1 \sin 2\alpha_3 \\ -\cos 2\alpha_2 \sin 2\alpha_3 & -(\sin 2\alpha_1 \sin 2\alpha_2 \sin 2\alpha_3 + \cos 2\alpha_1 \cos 2\alpha_3) & -(\cos 2\alpha_1 \sin 2\alpha_2 \sin 2\alpha_3 - \sin 2\alpha_1 \cos 2\alpha_3) \\ -\sin 2\alpha_2 & \sin 2\alpha_1 \cos 2\alpha_2 & \cos 2\alpha_1 \cos 2\alpha_3 \end{pmatrix}, \tag{11}$$

we have that

$$S_{\text{canon}} = \sqrt{2}\langle \mathbf{R}^\top(\alpha_1, \alpha_2, \alpha_3)\boldsymbol{x}_1 \cdot \hat{\boldsymbol{\sigma}} \otimes \mathbf{R}^\top(\beta_1, \beta_2, \beta_3)\boldsymbol{x}_1 \cdot \hat{\boldsymbol{\sigma}} + \mathbf{R}^\top(\alpha_1, \alpha_2, \alpha_3)\boldsymbol{x}_3 \cdot \hat{\boldsymbol{\sigma}} \otimes \mathbf{R}^\top(\beta_1, \beta_2, \beta_3)\boldsymbol{x}_3 \cdot \hat{\boldsymbol{\sigma}} \rangle. \tag{12}$$

Using Eq. (4) in Eq. (12) gives

$$S_{\text{canon}} = \sqrt{2}[\mathbf{R}^\top(\alpha_1, \alpha_2, \alpha_3)\boldsymbol{x}_1 \cdot \mathbf{T}\mathbf{R}^\top(\beta_1, \beta_2, \beta_3)\boldsymbol{x}_1 + \mathbf{R}^\top(\alpha_1, \alpha_2, \alpha_3)\boldsymbol{x}_3 \cdot \mathbf{T}\mathbf{R}^\top(\beta_1, \beta_2, \beta_3)\boldsymbol{x}_3]. \tag{13}$$

We now consider the polar decomposition of the matrix $\mathbf{T}$. That is, we consider a unitary matrix $\mathbf{W} = \mathbf{T}(\mathbf{T}^\top\mathbf{T})^{-1/2}$ and symmetric matrix $\sqrt{\mathbf{V}} = \sqrt{\mathbf{T}^\top\mathbf{T}}$ such that $\mathbf{T} = \mathbf{W}\sqrt{\mathbf{V}}$. Without loss of generality, we next choose the α_j such that $\mathbf{W}^\top\mathbf{R}^\top(\alpha_1, \alpha_2, \alpha_3) = \mathbf{R}^\top(\beta_1, \beta_2, \beta_3)$. This gives

$$S_{\text{canon}} = \sqrt{2}[\mathbf{R}^\top(\beta_1, \beta_2, \beta_3)\boldsymbol{x}_1 \cdot \sqrt{\mathbf{V}}\mathbf{R}^\top(\beta_1, \beta_2, \beta_3)\boldsymbol{x}_1 + \mathbf{R}^\top(\beta_1, \beta_2, \beta_3)\boldsymbol{x}_3 \cdot \sqrt{\mathbf{V}}\mathbf{R}^\top(\beta_1, \beta_2, \beta_3)\boldsymbol{x}_3]. \tag{14}$$

We now want use the angles β_j to optimize S_{canon}. This is a completely analogous optimization problem to that of Ref. [45]. We recall that the matrix $\mathbf{V}$ is symmetric. This means that the eigenvectors of $\mathbf{V}$ are orthogonal, allowing us to choose the β_j so that the vectors $\mathbf{R}^\top(\beta_1, \beta_2, \beta_3)\boldsymbol{x}_1$ and $\mathbf{R}^\top(\beta_1, \beta_2, \beta_3)\boldsymbol{x}_3$ are aligned to the eigenvectors corresponding to the two largest eigenvalues of $\mathbf{V}$. Following the same arguments of Ref. [45], we now have that the optimal value of S_{canon} is

$$S_{\text{canon}} = \sqrt{2}(\sqrt{v_1} + \sqrt{v_2}), \tag{15}$$

where v_1 and v_2 are once again the two leading eigenvalues of the matrix $\mathbf{V}$. Comparison of Eqs. (5) and (15) reveals that $S_{\text{canon}} \leqslant S_{\text{max}}$ in general as expected.

Equation (15) shows that the CHSH parameter with fixed Bell test angles depends on the same two parameters as the optimal CHSH parameter where the Bell test angles were allowed to vary. Since these parameters are positive, both S_{max} and S_{canon} are both monotonically dependent on the nonlocality of the underlying system. This relationship provides a useful technique in characterizing the impairments affecting a CHSH parameter measurement.

To see this, note that, like Ref. [45], we have not specified the optimization angles α_j and β_j that yield S_{canon}. As with S_{max}, finding the angles for a general state is an analytically hard problem. However, as mentioned above, this arrangement presupposes that the target state of a CHSH violation experiment is one of the four Bell states. These states have $\mathbf{V}$ matrices with eigenvectors that are automatically aligned to the unit vectors $\boldsymbol{x}_1$ and $\boldsymbol{x}_3$ or are rotated by $\pi/2$ about a known axis. Certain impairments either preserve this alignment or misalign each channel independently, allowing the optimization angles to be trivially obtained. Since each channel is affected independently and the parameter S_{canon} depends only on the optimization angles, which are local operations, we have transformed the optimization problem into an alignment problem. We may thus probe the system first with classical signals to find the ideal values for the optimization angles before any entangled resources are used in Fig. 1(b). These angles will be those that preserve the alignment of the classical signal in the two-qubit space of each channel after the signals have been subjected to the same impairments that would affect the entangled state. We will show specific examples of these impairments in the following section. With a method for easily computing S_{canon}, we now have a technique for experimentally characterizing the impairments affecting a general quantum system.

Thus far, we have made no assumptions about the state of the system after all qubit-preserving impairments have been considered, and Eqs. (5) and (15) are completely general. We will now demonstrate an interesting property of impairments that preserve the purity of the state. That is, we will assume that the target state is expected to be pure and the impairments affecting the system preserve $\text{Tr}(\hat{\rho}^2) = 1$.

Let a general pure state be defined using the state vector

$$|\psi\rangle = C_{00}|0\rangle \otimes |0\rangle + C_{01}|0\rangle \otimes |1\rangle + C_{10}|1\rangle \otimes |0\rangle + C_{11}|1\rangle \otimes |1\rangle, \tag{16}$$

where the C_{jk} are complex coefficients such that

$$|C_{00}|^2 + |C_{01}|^2 + |C_{10}|^2 + |C_{11}|^2 = 1. \tag{17}$$

The density operator corresponding to the pure state would be given as $\hat{\rho}_{\text{pure}} = |\psi\rangle\langle\psi|$. Expressing this density operator in the form of Eq. (4) gives a $\mathbf{T}$ matrix [45]

$$\mathbf{T}_{\text{pure}} = \begin{pmatrix} 2\text{Re}(C_{00}^* C_{11} + C_{01}^* C_{10}) & 2\text{Im}(C_{00}^* C_{11} - C_{01}^* C_{10}) & 2\text{Re}(C_{00}^* C_{10} - C_{11}^* C_{01}) \\ 2\text{Im}(C_{00}^* C_{11} + C_{01}^* C_{10}) & -2\text{Re}(C_{00}^* C_{11} - C_{01}^* C_{10}) & 2\text{Im}(C_{00}^* C_{10} + C_{11}^* C_{01}) \\ 2\text{Re}(C_{00}^* C_{01} - C_{11}^* C_{10}) & 2\text{Im}(C_{00}^* C_{01} + C_{11}^* C_{10}) & |C_{00}|^2 + |C_{11}|^2 - |C_{01}|^2 - |C_{10}|^2 \end{pmatrix}. \tag{18}$$

If we were to now compute the matrix $\mathbf{V}_{\text{pure}} = \mathbf{T}_{\text{pure}}^{\top}\mathbf{T}_{\text{pure}}$ we would find that its eigenvalues take on the remarkably simple form

$$\begin{aligned} v_1 &= 1 \\ v_2 = v_3 &= 4|C_{00}C_{11} - C_{01}C_{10}|^2. \end{aligned} \tag{19}$$

If we were to use Eq. (19) in either Eq. (5) or Eq. (15), we would find that the optimal CHSH parameter now only depends on a single free parameter. We refer to this parameter as the mismatch parameter γ and define it as

$$\gamma \equiv \sqrt{v_2} = 2|C_{00}C_{11} - C_{01}C_{10}|. \tag{20}$$

This parameter is identical to the nonlocality measure and entanglement measures for pure states as demonstrated in Ref. [33]. With this mismatch parameter, the maximum possible measurable CHSH parameter $S_{\max}$ for a pure state is given as

$$S_{\max} = 2\sqrt{1+\gamma^2}, \tag{21}$$

while the maximum possible measurable CHSH parameter with keeping the Bell test angles fixed to those of Eq. (6) S_{canon} for a pure state is simply

$$S_{\text{canon}} = \sqrt{2}(1+\gamma). \tag{22}$$

This means that all possible qubit-preserving impairments that reduce the CHSH parameter while preserving the purity of the state can be characterized by a single parameter γ. We see that this mismatch parameter can be easily obtained from Eq. (22). This demonstrates an additional advantage of Fig. 1(b) for pure states.

There exists a theoretical advantage for pure states as well. That is, we may simply obtain the mismatch parameter directly from the matrix $\mathbf{T}_{\text{pure}}$ as

$$\det(\mathbf{T}_{\text{pure}}) = -4|C_{00}C_{11} - C_{01}C_{10}|^2 = -\gamma^2, \tag{23}$$

where "det" denotes the determinant. Thus, we have that $\gamma = \sqrt{-\det(\mathbf{T}_{\text{pure}})}$.

Recall that certain impairments will preserve the alignment of the eigenvectors with the unit vectors $\boldsymbol{x}_1$ and $\boldsymbol{x}_3$. We now provide two examples where we may let $\alpha_j = \beta_j = 0$ for all $j \in \{1,2,3\}$. Such systems will have diagonal $\mathbf{V}$ matrices. We may then let their $\mathbf{T}$ matrices be diagonal so that the $\mathbf{T}$ matrices for the two examples are given as

$$\mathbf{T}_{\text{o}} = \begin{pmatrix} 1 & 0 & 0 \\ 0 & -\gamma & 0 \\ 0 & 0 & \gamma \end{pmatrix} \quad \text{and} \quad \mathbf{T}_{\text{u}} = \begin{pmatrix} \gamma & 0 & 0 \\ 0 & -\gamma & 0 \\ 0 & 0 & 1 \end{pmatrix}. \tag{24}$$

Inspection of Eq. (24) reveals that we may let $\alpha_j = \beta_j = 0$ for all $j \in \{1,2,3\}$ as described. The pure states corresponding to these two $\mathbf{T}$ matrices are

$$\begin{aligned} |\psi_{\text{o}}\rangle = \frac{1}{2}[&\sqrt{1+\gamma}(|0\rangle\otimes|0\rangle + |1\rangle\otimes|1\rangle) \\ &+ \sqrt{1-\gamma}(|0\rangle\otimes|1\rangle + |1\rangle\otimes|0\rangle)], \end{aligned}$$

$$\begin{aligned} |\psi_{\text{u}}\rangle = &\sqrt{\frac{1+\sqrt{1-\gamma^2}}{2}}|0\rangle\otimes|0\rangle \\ &+ \sqrt{\frac{1-\sqrt{1-\gamma^2}}{2}}|1\rangle\otimes|1\rangle. \end{aligned} \tag{25}$$

Using the fact that the four Bell states are given as

$$\begin{aligned} |\Phi^{\pm}\rangle &= \frac{1}{\sqrt{2}}(|0\rangle\otimes|0\rangle \pm |1\rangle\otimes|1\rangle), \\ |\Psi^{\pm}\rangle &= \frac{1}{\sqrt{2}}(|0\rangle\otimes|1\rangle \pm |1\rangle\otimes|0\rangle), \end{aligned} \tag{26}$$

we see that the mismatch parameter can affect the system in two distinct ways. That is, we obtain the superposition of two opposing Bell states, $|\psi_{\text{o}}\rangle$, or we have a single Bell state that is unbalanced, $|\psi_{\text{u}}\rangle$. These two situations are equivalent up to a local operation given by the optimization angles of Fig. 1(b). Furthermore, the optimization angles of Fig. 1(b) may transform any pure state to those of Eq. (25) up to a phase difference, which does not contribute a reduction to $S_{\max}$ or S_{canon}.

In this section, we introduced a generalized characterization of impairments affecting a CHSH measurement. We demonstrated that, by fixing the Bell test angles to those of Eq. (6), the resulting optimal CHSH parameter S_{canon} depends on the same free parameters as the truly optimal CHSH parameter $S_{\max}$. Furthermore for pure states, the number of possible free parameters that reduce the CHSH parameter drops from two to one. This free parameter was denoted as the mismatch parameter and is easily computed. The relationship between S_{canon} and $S_{\max}$ allows for easy computation of the optimal CHSH parameter regardless of the impairments affecting the underlying physical system.

III. EXAMPLE IMPAIRMENTS IN POLARIZATION-ENCODED QUBITS

In this section, we consider characterizing the impairments that can affect a CHSH experiment involving polarization-encoded qubits using the techniques of the previous section. Specifically, we are considering the physical situation outlined in Fig. 2. This experimental setup is designed to produce Bell states entangled in a photon's polarization degree of freedom.

If we let $|\mathbb{0}\rangle$ correspond to the optical vacuum state, then the qubit states of Eq. (1) can be represented as

$$|0\rangle = \hat{\mathsf{c}}_{\text{H}}^{\dagger}|\mathbb{0}\rangle, \quad |1\rangle = \hat{\mathsf{c}}_{\text{V}}^{\dagger}|\mathbb{0}\rangle, \tag{27}$$

where $\hat{\mathsf{c}}_{\text{H}}^{\dagger}$ creates a horizontally polarized photon and $\hat{\mathsf{c}}_{\text{V}}^{\dagger}$ creates a vertically polarized photon. To incorporate both spatial paths, we define

$$\hat{\mathsf{a}}_{\text{H,V}}^{\dagger} \equiv \hat{\mathsf{c}}_{\text{H,V}}^{\dagger}\otimes\hat{\mathbb{1}}, \quad \hat{\mathsf{b}}_{\text{H,V}}^{\dagger} \equiv \hat{\mathbb{1}}\otimes\hat{\mathsf{c}}_{\text{H,V}}^{\dagger}, \tag{28}$$

where the operators $\hat{\mathsf{a}}_{\text{H,V}}^{\dagger}$ act on path A and the operators $\hat{\mathsf{b}}_{\text{H,V}}^{\dagger}$ act on path B.

Ideally, the pumped PPKTP source in Fig. 2 produces a single pair of orthogonally polarized photons. This pair passes through a polarizing beam splitter and is recombined at a

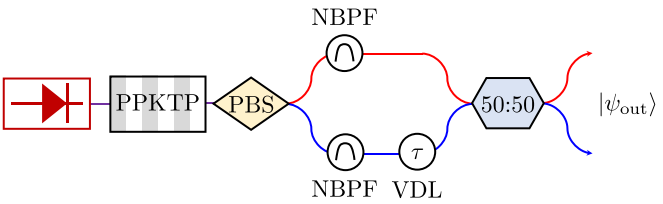

FIG. 2. A technique for generating the $|\Psi^-\rangle$ Bell state of Eq. (26) using the joint polarization state of a photon pair. A periodically poled potassium-titanyl-phosphate (PPKTP) crystal is pumped to produce orthogonally polarized photon pairs through the process of type-II spontaneous parametric down conversion (SPDC). The pairs are split at a polarizing beam splitter (PBS) and recombined at a 50:50 beam splitter to produce the state of Eq. (29) in the main text. Each of these components may be nonideal, contributing sources of impairments to the resulting CHSH parameter. Additionally, we have narrow bandpass filters (NBPF) and a variable delay line (VDL) that may contribute additional impairments if not properly aligned.

50:50 beam splitter to produce the state

$$|\psi\rangle = \tfrac{1}{2}(\hat{a}_H^\dagger \hat{b}_V^\dagger - \hat{a}_V^\dagger \hat{b}_H^\dagger + i\hat{a}_H^\dagger \hat{a}_V^\dagger + i\hat{b}_H^\dagger \hat{b}_V^\dagger)|\mathbb{0}\rangle. \tag{29}$$

Note that Eq. (29) contains terms that are outside of the two-qubit encoding of Eq. (4). These terms do not contribute any coincidence counts to the CHSH measurement and can be safely ignored when considering only qubit-preserving impairments. Normalizing this postselected state gives the $|\Psi^-\rangle$ state of Eq. (26) in the polarization-encoded basis of Eq. (27). Therefore, in the ideal case $S_{\text{canon}} = S_{\text{max}} = 2\sqrt{2}$, which is the maximum value permitted by quantum mechanics [30].

In reality, the experimental components would not be ideal and the measured CHSH parameter value would likely be reduced. In the following sections, we will consider various impairments that could affect the CHSH experiment when using polarization-encoded qubits. Each of the impairments that we consider can be classified as qubit preserving, which we will see represents a significant number of the possible nonidealities in polarization-based quantum optical systems.

A. Polarization misalignments

The first class of impairments that we consider are those that affect the polarization state of the photons directly. There are several nonideal experimental components that can introduce this impairment. Additionally, these impairments can take on two distinct forms, those that can be compensated for using the optimization angles of Fig. 1(b) and those that cannot.

The first type of polarization misalignment we consider is the kind that can be compensated for using the optimization angles. Specifically, we will consider the case where the polarization vector of the photons in each path are rotated so they are no longer optimal. The total polarization misalignment in path A can be represented by a rotation of angle δ_A about some arbitrary axis of the Bloch sphere, and the total polarization misalignment in path B is a potentially different rotation by angle δ_B. For simplicity, we will let the axis of both of these polarization rotations be about the $\boldsymbol{x}_2$ axis of the Bloch sphere. Similar results exist for rotations about other axes.

The rotation by angles δ_A and δ_B as described above transforms the relevant terms of Eq. (29) as

$$|\psi_{\text{out}}\rangle = \frac{1}{\sqrt{2}}[\sin(\delta_A - \delta_B)(\hat{a}_H^\dagger \hat{b}_H^\dagger + \hat{a}_V^\dagger \hat{b}_V^\dagger) + \cos(\delta_A - \delta_B)(\hat{a}_H^\dagger \hat{b}_V^\dagger - \hat{a}_V^\dagger \hat{b}_H^\dagger)]|\mathbb{0}\rangle. \tag{30}$$

At first glance, the state of Eq. (30) appears to be of the form of the opposing Bell state case of Eq. (25). However, we note that there is a crucial minus sign in the final term of Eq. (30). Thus, using Eq. (30) in Eq. (20) gives the mismatch parameter as $\gamma = 1$, which gives $S_{\text{canon}} = S_{\text{max}} = 2\sqrt{2}$.

This means that this type of mismatch is easily correctable. To see this, let the general mismatch in a single path be described by the unitary operator $\hat{\Delta}(\delta)$. This rotation is now applied about an arbitrary axis as originally described above. We also recall the transformation due to the optimization angles $\hat{U}(\alpha_1, \alpha_2, \alpha_3) \otimes \hat{U}(\beta_1, \beta_2, \beta_3)$. The general output state after considering both the impairments and the optimization angles is given as

$$\begin{aligned}|\psi_{\text{out}}\rangle &= \hat{U}(\alpha_1, \alpha_2, \alpha_3) \otimes \hat{U}(\beta_1, \beta_2, \beta_3)\hat{\Delta}(\delta_A) \otimes \hat{\Delta}(\delta_B)|\Psi^-\rangle \\ &= \hat{U}(\alpha_1, \alpha_2, \alpha_3)\hat{\Delta}(\delta_A) \otimes \hat{U}(\beta_1, \beta_2, \beta_3)\hat{\Delta}(\delta_B)|\Psi^-\rangle.\end{aligned} \tag{31}$$

This means that we may choose the α_j such that $\hat{U}(\alpha_1, \alpha_2, \alpha_3) = \hat{\Delta}^\dagger(\delta_A)$ and we similarly choose the β_j such that $\hat{U}(\beta_1, \beta_2, \beta_3) = \hat{\Delta}^\dagger(\delta_B)$. This restores the original $|\Psi^-\rangle$ Bell state yielding $S_{\text{canon}} = S_{\text{max}} = 2\sqrt{2}$.

This is a well-known feature of polarization alignment in polarization-encoded quantum optical systems. Furthermore, if the operators $\hat{\Delta}(\delta_A)$ and $\hat{\Delta}(\delta_B)$ are channel specific and independent of whether a quantum or classical signal is inserted, we may use a classical signal to probe these rotations and find the optimization angles. This is one of the advantages of Fig. 1(b) that was discussed in Sec. II. We expect that similar techniques exist for other qubit encodings.

Not all polarization misalignments can be compensated for using the optimization angles in Eq. (31). We now consider polarization misalignment in the generation of the state of Eq. (29). There are several experimental components that can introduce such nonidealities. For simplicity, we will consider a nonideal 50:50 beam splitter. Similar results exist when considering a nonideal PBS.

The application of the unitary evolution operator for a general spatial beam splitter $\hat{U}_{BS}$ to a state transforms the creation operators of Eq. (28) as

$$\begin{aligned}\hat{a}_{H,V}^\dagger &\to \hat{U}_{BS}\hat{a}_{H,V}^\dagger\hat{U}_{BS}^\dagger = \mathcal{T}_{H,V}\hat{a}_{H,V}^\dagger + i\mathcal{R}_{H,V}\hat{b}_{H,V}^\dagger, \\ \hat{b}_{H,V}^\dagger &\to \hat{U}_{BS}\hat{b}_{H,V}^\dagger\hat{U}_{BS}^\dagger = \mathcal{T}_{H,V}\hat{a}_{H,V}^\dagger + i\mathcal{R}_{H,V}\hat{a}_{H,V}^\dagger,\end{aligned} \tag{32}$$

where

$$\mathcal{T}_{H,V}^2 + \mathcal{R}_{H,V}^2 = 1. \tag{33}$$

Given this transformation, the generated state is not given by Eq. (29), but is instead given as

$$|\psi_{\text{out}}\rangle = \frac{1}{\sqrt{\mathcal{T}_H^2\mathcal{T}_V^2 + \mathcal{R}_H^2\mathcal{R}_V^2}}(\mathcal{T}_H\mathcal{T}_V\hat{a}_H^\dagger\hat{b}_V^\dagger - \mathcal{R}_H\mathcal{R}_V\hat{a}_V^\dagger\hat{b}_H^\dagger)|\mathbb{0}\rangle, \tag{34}$$

where we have neglected the terms that do not contribute coincidence counts and normalized the postselected state.

Inspection of Eq. (34) reveals that this output state is indeed of the form of the unbalanced Bell state example of Eq. (25). Using Eq. (34) in Eq. (20) gives the mismatch parameter as

$$\gamma = \frac{2\mathcal{T}_{\mathrm{H}}\mathcal{T}_{\mathrm{V}}\mathcal{R}_{\mathrm{H}}\mathcal{R}_{\mathrm{V}}}{\mathcal{T}_{\mathrm{H}}^2\mathcal{T}_{\mathrm{V}}^2 + \mathcal{R}_{\mathrm{H}}^2\mathcal{R}_{\mathrm{V}}^2}. \tag{35}$$

This parameter can then be used in Eqs. (21) and (22) to give $S_{\max}$ and S_{canon}, respectively. The ideal value of $\gamma = 1$, where $S_{\mathrm{canon}} = S_{\max} = 2\sqrt{2}$, occurs when $\mathcal{T}_{\mathrm{H}} = \mathcal{T}_{\mathrm{V}} = \mathcal{R}_{\mathrm{H}} = \mathcal{R}_{\mathrm{V}} = 1/\sqrt{2}$, corresponding to an ideal spatial 50:50 beam splitter as expected.

Note that the optimization angles do not need to be adjusted from the settings that give the ideal value for $|\Psi^-\rangle$ in this particular example. This confirms the argument for the versatility of S_{canon} introduced in the previous section. Furthermore, even when the optimization angles need to be adjusted, they often have a trivial relationship with a given nonideality such as in the polarization mismatch of Eq. (31).

B. Spectrotemporal impairments

The creation operators $\hat{\mathsf{c}}_{\mathrm{H}}^\dagger$ and $\hat{\mathsf{c}}_{\mathrm{V}}^\dagger$ of Eq. (27) approximately correspond to the creation of single-mode photons. Such photons can be said to have been created at a known time t or with a known angular frequency ω. However, in reality photons are distributed in creation time and likewise have a distribution of possible angular frequencies as required by the principles of quantum mechanics. Thus, the creation operators of Eq. (27) may be further specified as [47]

$$\hat{\mathsf{c}}_{\mathrm{H,V}}^\dagger = \int dt\, f_{\mathrm{H,V}}(t)\hat{\mathsf{C}}_{\mathrm{H,V}}(t) = \int d\omega \tilde{f}_{\mathrm{H,V}}(\omega)\tilde{\mathsf{C}}_{\mathrm{H,V}}(\omega), \tag{36}$$

where

$$\begin{aligned}[\hat{\mathsf{C}}_j(t), \hat{\mathsf{C}}_k^\dagger(t')] &= \delta_{j,k}\delta(t-t'),\\ [\tilde{\mathsf{C}}_j(\omega), \tilde{\mathsf{C}}_k^\dagger(\omega')] &= \delta_{j,k}\delta(\omega-\omega'),\end{aligned} \tag{37}$$

with $\delta(x)$ being the Dirac delta function, $\delta_{j,k}$ being the Kronecker delta function, $j, k \in \{\mathrm{H,V}\}$; and

$$\tilde{\mathsf{C}}_{\mathrm{H,V}}^\dagger(\omega) = \frac{1}{\sqrt{2\pi}}\int dt e^{i\omega t}\hat{\mathsf{C}}_{\mathrm{H,V}}^\dagger(t), \tag{38}$$

so that

$$\tilde{f}_{\mathrm{H,V}}(\omega) = \frac{1}{\sqrt{2\pi}}\int dt e^{-i\omega t}\mathsf{f}_{\mathrm{H,V}}(t). \tag{39}$$

The operators of Eq. (38) are known as the multimode creation operators.

Depending on the source of polarization-encoded photons, it may no longer be possible to simply express the operators $\hat{\mathsf{a}}_{\mathrm{H,V}}^\dagger$ and $\hat{\mathsf{b}}_{\mathrm{H,V}}^\dagger$ using Eq. (28). Instead, we would need to use the multimode creation operators

$$\begin{aligned}\hat{\mathsf{A}}_{\mathrm{H,V}}^\dagger(t) &\equiv \hat{\mathsf{C}}_{\mathrm{H,V}}^\dagger(t)\otimes\hat{\mathbb{1}}, \quad \tilde{\mathsf{A}}_{\mathrm{H,V}}^\dagger(\omega) \equiv \tilde{\mathsf{C}}_{\mathrm{H,V}}^\dagger(\omega)\otimes\hat{\mathbb{1}},\\ \hat{\mathsf{B}}_{\mathrm{H,V}}^\dagger(t) &\equiv \hat{\mathbb{1}}\otimes\hat{\mathsf{C}}_{\mathrm{H,V}}^\dagger(t), \quad \tilde{\mathsf{B}}_{\mathrm{H,V}}^\dagger(\omega) \equiv \hat{\mathbb{1}}\otimes\tilde{\mathsf{C}}_{\mathrm{H,V}}^\dagger(\omega)\end{aligned} \tag{40}$$

to define [47]

$$\begin{aligned}\hat{\mathsf{a}}_j^\dagger\hat{\mathsf{b}}_k^\dagger &= \int dt_{\mathrm{A}}dt_{\mathrm{B}}F_{jk}(t_{\mathrm{A}},t_{\mathrm{B}})\hat{\mathsf{A}}_j^\dagger(t_{\mathrm{A}})\hat{\mathsf{B}}_k^\dagger(t_{\mathrm{B}})\\ &= \int d\omega_{\mathrm{A}}d\omega_{\mathrm{B}}\tilde{F}_{jk}(\omega_{\mathrm{A}},\omega_{\mathrm{B}})\tilde{\mathsf{A}}_j^\dagger(\omega_{\mathrm{A}})\tilde{\mathsf{B}}_k^\dagger(\omega_{\mathrm{B}}),\end{aligned} \tag{41}$$

where $j, k \in \{\mathrm{H,V}\}$. The reason for this is due to the potential spectrotemporal entanglement present in the source photons. Such entanglement requires that the distributions $F_{\mathrm{H,V}}$ and $\tilde{F}_{\mathrm{H,V}}$ are nonseparable, meaning we cannot express the creation operators using Eq. (28). This gives the most general output pure state in the expanded spectrotemporal two-qubit basis as

$$\begin{aligned}|\psi_{\mathrm{out}}\rangle = \int dt_{\mathrm{A}}dt_{\mathrm{B}}[&F_{\mathrm{HH}}(t_{\mathrm{A}},t_{\mathrm{B}})\hat{\mathsf{A}}_{\mathrm{H}}^\dagger(t_{\mathrm{A}})\hat{\mathsf{B}}_{\mathrm{H}}^\dagger(t_{\mathrm{B}})\\ &+ F_{\mathrm{HV}}(t_{\mathrm{A}},t_{\mathrm{B}})\hat{\mathsf{A}}_{\mathrm{H}}^\dagger(t_{\mathrm{A}})\hat{\mathsf{B}}_{\mathrm{V}}^\dagger(t_{\mathrm{B}})\\ &+ F_{\mathrm{VH}}(t_{\mathrm{A}},t_{\mathrm{B}})\hat{\mathsf{A}}_{\mathrm{V}}^\dagger(t_{\mathrm{A}})\hat{\mathsf{B}}_{\mathrm{H}}^\dagger(t_{\mathrm{B}})\\ &+ F_{\mathrm{VV}}(t_{\mathrm{A}},t_{\mathrm{B}})\hat{\mathsf{A}}_{\mathrm{H}}^\dagger(t_{\mathrm{A}})\hat{\mathsf{B}}_{\mathrm{H}}^\dagger(t_{\mathrm{B}})]|\mathbb{0}\rangle.\end{aligned} \tag{42}$$

This state includes all possible impairments—spectrotemporal or otherwise—in the F_{jk} distributions that preserve the purity of the state. A similar formalism may be used to incorporate mixed states.

In quantum optics, each creation time and spectral frequency correspond to an independent mode. This is enforced by the commutation relationship of Eq. (37). This may seem to imply that spectrotemporal impairments are not qubit preserving because it requires expanding the qubit space to a continuum of modes as in Eq. (42). However, we let the computational basis still be described by Eq. (27) using the operators of Eq. (36). In this case, the distributions $f_{\mathrm{H,V}}(t)$ become detection window amplitudes and the distributions $\tilde{f}_{\mathrm{H,V}}(\omega)$ become spectral bandwidth amplitudes. We may continue to use the techniques of Sec. II; however, we need to demonstrate how the optimal CHSH parameters $S_{\max}$ and S_{canon} must be computed in this situation.

To begin, we note that one cannot directly measure projectors of the basis states in the computational basis of Eq. (27) when the operators are spectrotemporally defined by Eq. (36). Quantum optically we measure product intensities R of the form

$$\begin{aligned}R_{jk} &= \int dt_{\mathrm{A}}dt_{\mathrm{B}}\langle\hat{\mathsf{A}}_j^\dagger(t_{\mathrm{A}})\hat{\mathsf{A}}_j(t_{\mathrm{A}})\hat{\mathsf{B}}_k^\dagger(t_{\mathrm{B}})\hat{\mathsf{B}}_k(t_{\mathrm{B}})\rangle\\ &= \int d\omega_{\mathrm{A}}d\omega_{\mathrm{B}}\langle\tilde{\mathsf{A}}_j^\dagger(\omega_{\mathrm{A}})\tilde{\mathsf{A}}_j(\omega_{\mathrm{A}})\tilde{\mathsf{B}}_k^\dagger(\omega_{\mathrm{B}})\tilde{\mathsf{B}}_k(\omega_{\mathrm{B}})\rangle,\end{aligned} \tag{43}$$

where $j, k \in \{\mathrm{H,V}\}$. The R_{jk} of Eq. (43) are proportional to coincidence rates, which can be used to define the measurable CHSH parameter. This fact inspires the definition of the following set of operators:

$$\begin{aligned}\hat{\Sigma}_1(t) &\equiv \hat{\mathsf{C}}_{\mathrm{H}}^\dagger(t)\hat{\mathsf{C}}_{\mathrm{V}}(t) + \hat{\mathsf{C}}_{\mathrm{V}}^\dagger(t)\hat{\mathsf{C}}_{\mathrm{H}}(t),\\ \hat{\Sigma}_2(t) &\equiv i\hat{\mathsf{C}}_{\mathrm{H}}^\dagger(t)\hat{\mathsf{C}}_{\mathrm{V}}(t) - i\hat{\mathsf{C}}_{\mathrm{V}}^\dagger(t)\hat{\mathsf{C}}_{\mathrm{H}}(t),\\ \hat{\Sigma}_3(t) &\equiv \hat{\mathsf{C}}_{\mathrm{H}}^\dagger(t)\hat{\mathsf{C}}_{\mathrm{H}}(t) - \hat{\mathsf{C}}_{\mathrm{V}}^\dagger(t)\hat{\mathsf{C}}_{\mathrm{V}}(t),\end{aligned} \tag{44}$$

with similar definitions for a set $\tilde{\Sigma}_j(\omega)$ $j \in \{1,2,3\}$ using the operators $\tilde{\mathsf{C}}_k^\dagger(\omega)$ $k \in \{\mathrm{H,V}\}$. The operators of Eq. (44) are

averaged over all times to give measurements of the Pauli operators in polarization-encoded quantum-optical systems. Such measurements are used to define the corresponding CHSH parameter using expressions such as Eq. (7) or the techniques of Ref. [45].

We now find the optimal CHSH parameters $S_{\max}$ and S_{canon}. Since the only usable information comes from the time-averaged measurements of the observables of Eq. (44) in polarization-encoded quantum-optical systems, we may now define an effective $\mathbf{T}$ matrix with elements

$$\begin{aligned} T_{jk} &\equiv \int dt_{\mathrm{A}} dt_{\mathrm{B}} \langle \hat{\Sigma}_j(t_{\mathrm{A}}) \otimes \hat{\Sigma}_k(t_{\mathrm{B}}) \rangle \\ &= \int d\omega_{\mathrm{A}} d\omega_{\mathrm{B}} \langle \tilde{\Sigma}_j(\omega_{\mathrm{A}}) \otimes \tilde{\Sigma}_k(\omega_{\mathrm{B}}) \rangle, \end{aligned} \tag{45}$$

where $j, k \in \{1, 2, 3\}$, and we may once again use the arguments of Sec. II. That is, $S_{\max}$ is given by Eq. (5) and S_{canon} is given by Eq. (15). This is only true if the state is given by Eq. (42), its equivalent mixed state definition, or includes negligible terms that do not contribute coincidence counts. Otherwise, we would have an impairment that is not qubit preserving.

Defining the effective matrix of Eq. (45) with similarly defined Bloch vectors $\boldsymbol{a}$ and $\boldsymbol{b}$ yields effective density operators through Eq. (4). However, this effective density operator can correspond to a mixed state even when the actual state is pure. That is, if the state is given by the pure state of Eq. (42), the effective two-qubit density operator of Eq. (4) may be a mixed state depending on the distributions F_{jk} $j, k \in \{\mathrm{H}, \mathrm{V}\}$. This state is mixed by the averaged measurement of the observables of Eq. (44). This means that we cannot define a mismatch parameter using Eq. (20) in this situation. Despite this fact, if we consider only the spectral impairments in the experiment of Fig. 2, and neglect all other types of impairments, the output state simplifies to

$$\begin{aligned} |\psi\rangle &= \frac{1}{\sqrt{2}} \int dt_{\mathrm{A}} dt_{\mathrm{B}} [F_0(t_{\mathrm{A}}, t_{\mathrm{B}}) \hat{\mathsf{A}}_{\mathrm{H}}^{\dagger}(t_{\mathrm{A}}) \hat{\mathsf{B}}_{\mathrm{V}}^{\dagger}(t_{\mathrm{B}}) \\ &\quad - F_0(t_{\mathrm{B}}, t_{\mathrm{A}}) \hat{\mathsf{A}}_{\mathrm{V}}^{\dagger}(t_{\mathrm{A}}) \hat{\mathsf{B}}_{\mathrm{H}}^{\dagger}(t_{\mathrm{B}})] |\mathbb{0}\rangle \\ &= \frac{1}{\sqrt{2}} \int d\omega_{\mathrm{A}} d\omega_{\mathrm{B}} [\tilde{F}_0(\omega_{\mathrm{A}}, \omega_{\mathrm{B}}) \tilde{\mathsf{A}}_{\mathrm{H}}^{\dagger}(\omega_{\mathrm{A}}) \tilde{\mathsf{B}}_{\mathrm{V}}^{\dagger}(\omega_{\mathrm{B}}) \\ &\quad - \tilde{F}_0(\omega_{\mathrm{B}}, \omega_{\mathrm{A}}) \tilde{\mathsf{A}}_{\mathrm{V}}^{\dagger}(\omega_{\mathrm{A}}) \hat{\mathsf{B}}_{\mathrm{H}}^{\dagger}(\omega_{\mathrm{B}})] |\mathbb{0}\rangle, \end{aligned} \tag{46}$$

where the distribution F_0 is normalized over all times or $\tilde{F}_0$ is equivalently normalized over all angular frequencies, and they contain all spectrotemporal impairments. Ideally, $F_0(t_{\mathrm{A}}, t_{\mathrm{B}}) = F_0(t_{\mathrm{B}}, t_{\mathrm{A}})$ and $\tilde{F}_0(\omega_{\mathrm{A}}, \omega_{\mathrm{B}}) = \tilde{F}_0(\omega_{\mathrm{B}}, \omega_{\mathrm{A}})$; however, spectrotemporal impairments such as misaligned filters and chromatic dispersion can cause this to not be the case. Using the state of Eq. (46) in Eq. (45) gives an effective $\mathbf{T}$ matrix with a corresponding matrix $\mathbf{V} = \mathbf{T}^{\top}\mathbf{T}$ that has eigenvalues $v_1 = 1$ and $v_2 = v_3 = \gamma$, where

$$\begin{aligned} \gamma &= \int dt_{\mathrm{A}} dt_{\mathrm{B}} F_0^*(t_{\mathrm{B}}, t_{\mathrm{A}}) F_0(t_{\mathrm{A}}, t_{\mathrm{B}}) \\ &= \int d\omega_{\mathrm{A}} d\omega_{\mathrm{B}} \tilde{F}_0^*(\omega_{\mathrm{B}}, \omega_{\mathrm{A}}) \tilde{F}_0(\omega_{\mathrm{A}}, \omega_{\mathrm{B}}), \end{aligned} \tag{47}$$

which is a single effective mismatch parameter. Thus, the effective density operator is pure in this case and the optimal CHSH parameters $S_{\max}$ and S_{canon} are given by Eqs. (21) and (22), respectively. This is an analogous result to that of Ref. [48].

In this section, we demonstrated how spectrotemporal impairments may be incorporated into the optimal CHSH parameters of Sec. II. This involves defining an effective $\mathbf{T}$ matrix using Eqs. (44) and (45). When incorporating both spectrotemporal impairments and the polarization impairments of the previous section, this effective $\mathbf{T}$ matrix can correspond to a mixed state even if the actual state is otherwise pure. However, if we only consider spectrotemporal impairments in the experiment of Fig. 2, we find that the effective state is also pure and we may define an effective mismatch parameter using Eq. (47).

C. White noise

For the final example, we consider a nonideal system subject to noise. Specifically, we will consider a model for white noise given as

$$\hat{\rho}_{\text{out}} = \eta |\psi_{\text{out}}\rangle\langle\psi_{\text{out}}| + \frac{1-\eta}{4} \hat{\mathbb{1}} \otimes \hat{\mathbb{1}}, \tag{48}$$

where $|\psi_{\text{out}}\rangle$ is a state subject to impairments. For simplicity, we will ignore spectral impairments in this situation. Furthermore, white noise is an important type of noise to consider in polarization-encoded systems since the noise part of the state represents completely unpolarized light.

If the state $|\psi_{\text{out}}\rangle = |\Psi^-\rangle$, we have a Werner state [49]. We will thus assume that the ideal state is the pure state $|\Psi^-\rangle$. Additionally, the density operator $\hat{\rho} = \hat{\mathbb{1}} \otimes \hat{\mathbb{1}}/4$ is the maximally mixed state. Therefore, if we define a unitary evolution operator $\hat{\mathsf{U}}_{\text{imp}}$ that describes all impairments that preserve the purity of the state, then we have

$$\tfrac{1}{4} \hat{\mathsf{U}}_{\text{imp}} \hat{\mathbb{1}} \otimes \hat{\mathbb{1}} \hat{\mathsf{U}}_{\text{imp}}^{\dagger} = \tfrac{1}{4} \hat{\mathbb{1}} \otimes \hat{\mathbb{1}}, \tag{49}$$

meaning we can consider the noise and all other impairments separately. However, Eq. (48) is not the only noise model that exists [33,34], and it is possible to have noise that couples to impairments. In these situations, Eqs. (5) and (15) still hold, and we consider the model of Eq. (48) for simplicity.

Another advantage of Eq. (49) is that the optimization angles for S_{canon} do not affect the noise part of the density operator. This means that we can let $|\psi_{\text{out}}\rangle$ be given by one of the two states of Eq. (25) without loss of generality. Using the $|\psi_{\mathrm{o}}\rangle$ of Eq. (25) as $|\psi_{\text{out}}\rangle$ in Eq. (48) and inserting the result into Eq. (4) gives a $\mathbf{T}$ matrix as

$$\mathbf{T} = \begin{pmatrix} \eta & 0 & 0 \\ 0 & -\eta\gamma & 0 \\ 0 & 0 & \eta\gamma \end{pmatrix}. \tag{50}$$

Trivially, computing $\mathbf{V} = \mathbf{T}^{\top}\mathbf{T}$ gives $v_1 = \eta^2$ and $v_2 = v_3 = \eta^2\gamma^2$. Thus, the optimal CHSH parameter of Fig. 1(a) is

$$S_{\max} = 2\eta\sqrt{1+\gamma^2}, \tag{51}$$

and the optimal CHSH parameter of Fig. 1(b) is

$$S_{\text{canon}} = \sqrt{2}\eta(1+\gamma). \tag{52}$$

From $S_{\max}$ and S_{canon} we see that noise part and the mismatch part in the reduction of the optimal CHSH parameters of Figs. 1(a) and 1(b) are factorable as expected. As mentioned, this is only true for non-spectrally-dependent qubit-preserving impairments and a noise model of the form of Eq. (48). Nonetheless, this is still a useful result that allows for the characterization of white noise and other impairments of a system.

IV. CONCLUSION

In this paper, we demonstrated a method for experimentally characterizing the reductions to the maximum possible measurable CHSH parameter. This technique was independent of the underlying physical qubit encoding and only assumes that all impairments in the system are qubit preserving. Furthermore, we developed a simple technique for finding these reductions to the optimal CHSH parameter. This was by the use of the experiment in Fig. 1(b). This setup converts the complicated optimization procedure of Fig. 1(a) to a simple alignment problem using classical signals that yield the optimization angles in Fig. 1(b). Implementing the transformation due to these angles yields the CHSH parameter S_{canon} of Eq. (15). This parameter can then be related to the truly optimal CHSH parameter $S_{\max}$ using Eq. (5). For impairments that preserve the purity of the state, these expressions simplify further to Eqs. (22) and (21), respectively. Additionally, the experiment of Fig. 1(b) is able to discern the quality of entanglement using less measurements than full quantum state tomography.

We also demonstrated example impairments for the case of qubits encoded in the polarization degree of freedom in a quantum optical system. These examples demonstrated the usefulness of this characterization technique. Furthermore, we also developed a method in which spectral impairments may be incorporated into this formalism. This was by defining the effective **T** matrix of Eq. (45).

The techniques of this work are important in characterizing the quality of an entanglement resource in a quantum optical system. Entanglement is a vital resource in quantum information for the reasons specified in Sec. I. With the techniques introduced here, we hope to aid in system design. Characterizing impairments in this way allows for simplifying the process of finding the sources of detrimental impairments in a quantum system, and mitigating the effects of these impairments.

ACKNOWLEDGMENT

The authors acknowledge financial support from the US Department of Defense (DOD) Contract No. H98230-19-D-0003/0017.

[1] A. Einstein, B. Podolsky, and N. Rosen, Can quantum-mechanical description of physical reality be considered complete? Phys. Rev. **47**, 777 (1935).

[2] R. Horodecki, P. Horodecki, M. Horodecki, K. Horodecki, Quantum entanglement, Rev. Mod. Phys. **81**, 865 (2009).

[3] O. Gühne and G. Tóth, Entanglement detection, Phys. Rep. **474**, 1 (2009).

[4] A. K. Ekert, Quantum Cryptography Based on Bell's Theorem, Phys. Rev. Lett. **67**, 661 (1991).

[5] C. H. Bennett, G. Brassard, C. Crépeau, R. Jozsa, A. Peres, and W. K. Wootters, Teleporting an Unknown Quantum State via Dual Classical and Einstein-Podolsky-Rosen Channels, Phys. Rev. Lett. **70**, 1895 (1993).

[6] B. Yurke and D. Stoler, Bell's-inequality experiments using independent-particle sources, Phys. Rev. A **46**, 2229 (1992).

[7] D. E. Deutch, Quantum computational networks, Proc. R. Soc. London A **425**, 73 (1989).

[8] A. Barenco, C. H. Bennett, R. Cleve, D. P. DiVincenzo, N. Margolus, P. Shor, T. Sleator, J. A. Smolin, and H. Weinfurter, Elementary gates for quantum computation, Phys. Rev. A **52**, 3457 (1995).

[9] M. A. Nielsen and I. L. Chuang, *Quantum Computation and Quantum Information* (Cambridge University Press, Cambridge, 2000).

[10] A. Peres, Separability Criterion for Density Matrices, Phys. Rev. Lett. **77**, 1413 (1996).

[11] M. Horodecki, P. Horodecki, and R. Horodecki, Separability of mixed states: Necessary and sufficient conditions, Phys. Lett. A **223**, 1 (1996).

[12] C. H. Bennett, D. P. DiVincenzo, J. A. Smolin, and W. K. Wootters, Mixed-state entanglement and quantum error correction, Phys. Rev. A **54**, 3824 (1996).

[13] V. Vedral, M. B. Plenio, M. A. Rippin, and P. L. Knight, Quantifying Entanglement, Phys. Rev. Lett. **78**, 2275 (1997).

[14] W. K. Wootters, Entanglement of Formation of an Arbitrary State of Two Qubits, Phys. Rev. Lett. **80**, 2245 (1998).

[15] G. G. Stokes, On the composition and resolution of streams of polarized light from different sources, Trans. Cambridge Philos. Soc. **9**, 399 (1852).

[16] D. F. V. James, P. G. Kwiat, W. J. Munro, and A. G. White, Measurement of qubits, Phys. Rev. A **64**, 052312 (2001).

[17] B. M. Terhal, Bell inequalities and the separability criterion, Phys. Lett. A **271**, 319 (2000).

[18] M. Lewenstein, B. Kraus, J. I. Cirac, and P. Horodecki, Optimization of entanglement witnesses, Phys. Rev. A **62**, 052310 (2000).

[19] P. Horodecki, From limits of quantum operations to multicopy entanglement witnesses and state-spectrum estimation, Phys. Rev. A **68**, 052101 (2003).

[20] O. Gühne, P. Hyllus, D. Bruß, A. Ekert, M. Lewenstein, C. Macchiavello, and A. Sanpera, Detection of entanglement with few local measurements, Phys. Rev. A **66**, 062305 (2002).

[21] M. Barbieri, F. De Martini, G. Di Nepi, P. Mataloni, G. M. D'Ariano, and C. Macchiavello, Detection of Entanglement with Polarized Photons: Experimental Realization of an Entanglement Witness, Phys. Rev. Lett. **91**, 227901 (2003).

[22] O. Gühne and N. Lütkenhaus, Nonlinear Entanglement Witnesses, Phys. Rev. Lett. **96**, 170502 (2006).

[23] L. Rudnicki, P. Horodecki, and K. Zyczkowski, Collective Uncertainty Entanglement Test, Phys. Rev. Lett. **107**, 150502 (2011).
[24] S. Popescu, Bell's Inequalities and Density Matrices: Revealing "Hidden" Nonlocality, Phys. Rev. Lett. **74**, 2619 (1995).
[25] R. Horodecki, Two-spin-1/2 mixtures and Bell's inequalities, Phys. Lett. A **210**, 223 (1996).
[26] N. Brunner, D. Cavalcanti, S. Pironio, V. Scarani, and S. Wehner, Bell nonlocality, Rev. Mod. Phys. **86**, 419 (2014).
[27] J. S. Bell, On the Einstein Podolsky Rosen paradox, Phys. Phys. Fiz. **1**, 195 (1964).
[28] J. F. Clauser, M. A. Horne, A. Shimony, and R. A. Holt, Proposed Experiment to Test Local Hidden-Variable Theories, Phys. Rev. Lett. **23**, 880 (1969).
[29] G. Jaeger, *Quantum Information* (Springer Science+Business Media, New York, 2007).
[30] B. S. Cirel'son, Quantum generalizations of Bell's inequality, Lett. Math. Phys. **4**, 93 (1980).
[31] M. Giustina, M. A. M. Versteegh, S. Wengerowsky, J. Handsteiner, A. Hochrainer, K. Phelan, F. Steinlechner, J. Kofler, J. A. Larsson, C. Abellan, W. Amaya, V. Pruneri, M. W. Mitchell, J. Beyer, T. Gerrits, A. E. Lita, L. K. Shalm, S. W. Nam, T. Scheidl, R. Ursin *et al.* Significant-Loophole-Free Test of Bell's Theorem with Entangled Photons, Phys. Rev. Lett. **115**, 250401 (2015).
[32] N. Gisin, Bell's inequality holds for all non-product states, Phys. Lett. A **154**, 201 (1991).
[33] B. Horst, K. Bartkiewicz, and A. Miranowicz, Two-qubit mixed states more entangled than pure states: Comparison of the relative entropy of entanglement for a given nonlocality, Phys. Rev. A **87**, 042108 (2013).
[34] K. Bartkiewicz, B. Horst, K. Lemr, and A. Miranowicz, Entanglement estimation from Bell inequality violation, Phys. Rev. A **88**, 052105 (2013).
[35] T. Moroder, J.-D. Bancal, Y.-C. Liang, M. Hofmann, and O. Gühne, Device-Independent Entanglement Quantification and Related Applications, Phys. Rev. Lett. **111**, 030501 (2013).
[36] R. Horodecki, M. Horodecki, and P. Horodecki, Teleportation, Bell's inequalities and inseparability, Phys. Lett. A **222**, 21 (1996).
[37] N. Gisin and H. Bechmann-Pasquinucci, Bell inequality, Bell states and maximally entangled states for n qubits, Phys. Lett. A **246**, 1 (1998).
[38] Z. Chen, Bell-Klyshko Inequalities to Characterize Maximally Entangled States of n Qubits, Phys. Rev. Lett. **93**, 110403 (2004).
[39] B. Bellomo, R. Lo Franco, and G. Compagno, An optimized Bell test in a dynamical system, Phys. Lett. A **374**, 3007 (2010).
[40] Y. C. Ma and M. H. Yung, Transforming Bell's inequalities into state classifiers with machine learning, npj Quantum Inf. **4**, 34 (2018).
[41] A. A. Melnikov, P. Sekatski, and N. Sangouard, Setting Up Experimental Bell Tests with Reinforcement Learning, Phys. Rev. Lett. **125**, 160401 (2020).
[42] H. Takesue and K. Inoue, 1.5-μm band quantum-correlated photon pair generation in dispersion-shifted fiber: Suppression of noise photons by cooling fiber, Opt. Express **13**, 7832 (2005).
[43] H. Takesue and K. Shimizu, Effects of multiple pairs on visibility measurements of entangled photons generated by spontaneous parametric processes, Opt. Commun. **283**, 276 (2010).
[44] R. A. Brewster, G. Baumgartner, and Y. K. Chembo, Quantum analysis of polarization entanglement degradation induced by multiple-photon-pair generation, Phys. Rev. A **104**, 022411 (2021).
[45] R. Horodecki, P. Horodecki, and M. Horodecki, Violating Bell inequality by mixed spin-1/2 states: Necessary and sufficient condition, Phys. Lett. A **200**, 340 (1995).
[46] A. Milne, D. Jennings, and T. Rudolph, Geometric representation of two-qubit entanglement witnesses, Phys. Rev. A **92**, 012311 (2015).
[47] R. Loudon, *The Quantum Theory of Light*, 3rd ed. (Oxford University Press, Oxford, 1973).
[48] R. A. Brewster, J. Goldhar, M. Morris, G. Baumgartner, and Y. K. Chembo, Estimation of the CHSH parameter using HOM interference, IEEE Transactions on Quantum Engineering **3**, 4100310 (2022).
[49] R. F. Werner, Quantum states with Einstein-Podolsky-Rosen correlations admitting a hidden-variable model, Phys. Rev. A **40**, 4277 (1989).